Sequence-Inversion-Keyed Optical CDMA Coding/Decoding Scheme Using an Electrooptic Phase Modulator and Fiber Bragg Grating Arrays

Fei Zeng, *Member, IEEE*, Qing Wang, and Jianping Yao, *Senior Member, IEEE*

***Abstract*—We propose a novel approach for implementing unipolar-encoding/bipolar-decoding for optical code division multiple access (CDMA). In the proposed system, an electrooptic phase modulator (EOPM) and two fiber Bragg grating (FBG) arrays are employed. At the transmitter, a low-bit-rate data sequence modulates the phase of optical carriers by the EOPM, and is then wavelength-mapped to a high-bit-rate optical phase sequence by the encoder FBG array in a unipolar way. At the receiver, the second FBG array acts as a series of frequency discriminators to convert the phase-modulated optical signals to intensity-modulated signals, as well as a matched filter to perform optical decoding. Bipolar decoding is achieved by locating the optical carriers at either the positive or the negative slopes of the reflection responses of the decoder. The proposed encoding/decoding scheme is equivalent to a sequence-inversion-keyed (SIK) CDMA, which has the potential to provide an improved performance compared with the conventional incoherent scheme using optical orthogonal codes. Both theoretical and experimental studies of the proposed SIK scheme are presented.**

***Index Terms*—Electrooptic phase modulation, fiber Bragg grating, frequency discrimination, matched filter, optical code division multiple-access (CDMA), optical communications, optical signal processing, sequence inversion keying (SIK).**

I. Introduction

CDMA is one of the spread spectrum techniques that transmits data signals over a much larger bandwidth than a conventional transmission system; thus, it is particularly suited for optical fiber transmission networks where bandwidth is no longer a limited resource [1], [2]. However, for this resource to be utilized effectively, all-optical processing such as all-optical encoding and decoding must be used to avoid extra electrical to optical conversions. In addition, optical networks using all-optical processing can maintain a high data rate, which would not suffer from the electrical processing bottlenecks.

Optical CDMA can be implemented based on incoherent or coherent operation. For an incoherent optical CDMA, unipolar codes are utilized with matched filtering and direct detection at the receiver [3]–[5]. These so-called incoherent implementations provide the impetus for the development of unipolar pseudoorthogonal codes (0, 1). Compared with the conventional electronic bipolar codes $(-1, +1)$ such as Gold sequences, the cross-correlation function of unipolar codes is high and the number of codes in the family is very limited. Thus, long and sparse codes with narrower pulses have to be employed to support a larger number of users and higher transmission capacities, which is traded off against the complexity of the implementation. In a coherent optical CDMA, both the channel and reference sequences are required to be mapped to have a bipolar format, and signal-processing elements that are capable of distinguishing phase information should be used. The systems using coherent matched filters to manipulate optical phase have been reported by some researchers [6], [7]. In [6], Andonovic *et al*. proposed to achieve optical phase encoding and decoding using a pair of electrooptic phase modulators (EOPMs): one is at the transmitter end and the other is at the receiver end. However, the coding sequences employed to drive the modulators have to be electrically generated; therefore, the maximum achievable bit rate is limited by the speed of the electronic circuitry. Lam *et al*. [7] proposed a coherent temporally coded optical CDMA system based on ladder encoder/decoder. Limited by the geometry of ladder encoders, however, only few codes are available. The major disadvantage of the coherent approaches is the environmental influence and the polarization drift, rendering the coherent approach difficult to implement. A new family of optical CDMA systems based on bipolar modulation/balanced detection has been developed to improve the signal-to-noise ratio (SNR) [8]–[10]. Basically, the bipolar operation is realized by separating a bipolar sequence into two complementary unipolar sequences and performing unipolar-unipolar correlation in a pair of parallel correlators. The optical outputs of the correlators are subtracted at the receiver by a balanced photodetector (PD). Although such a scheme can perfectly cancel out the multiple-access interference (MAI) under an ideal situation, it brings a challenging implementation issue: additional complexity and cost at both the transmitter and the receiver.

On the other hand, a good compromise between the system complexity and performance can be achieved if the sequence inversion keying (SIK) scheme is used. In an SIK scheme, a unipolar channel sequence (0, 1) is correlated with a bipolar reference sequence $(-1, +1)$, which provides a better performance than an incoherent CDMA system but with a simpler architecture than a coherent CDMA system [11]. To compare the correlation performance between an SIK and an incoherent scheme, Gold codes of length 31 are employed since they are a popular choice in conventional CDMA systems. As shown in Fig. 1(a), two orthogonal Gold sequences are generated from a

Manuscript received December 1, 2006; revised March 7, 2006. This work was supported by the Natural Sciences and Engineering Research Council of Canada.

The authors are with the Microwave Photonics Research Laboratory, School of Information Technology and Engineering, University of Ottawa, Ottawa, ON K1N6N5, Canada (e-mail: fzeng@mit.edu; qingwang@site.uottawa.ca; jpyao@site.uottawa.ca).

Digital Object Identifier 10.1109/JSTQE.2007.897604

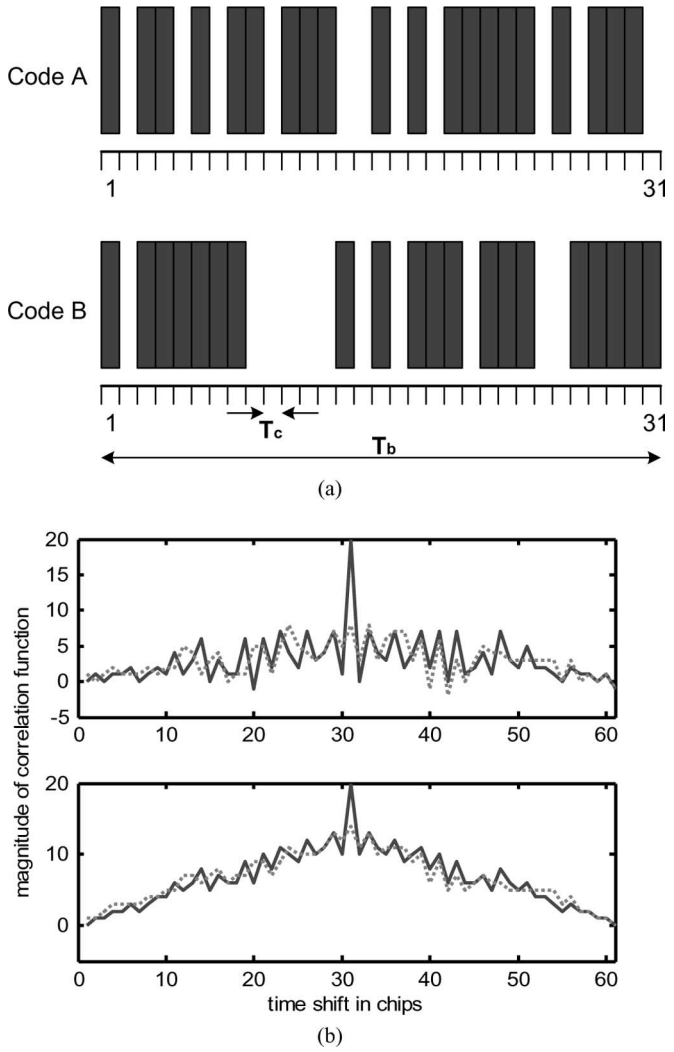

Fig. 1. Performance comparison between an incoherent (unipolar–unipolar) scheme and an SIK (unipolar–bipolar) scheme. a) Two Gold sequences of length 31: Code A and Code B. b) Comparison of autocorrelation (solid line) and cross-correlation (dotted line) functions for the two Gold codes: (upper) in an SIK system, (lower) in an incoherent system.

pair of maximum-length sequences where T_c and T_b represent the time durations of a chip and a data bit, respectively. Fig. 1(b) shows the autocorrelation and cross-correlation functions obtained for the SIK and incoherent systems, respectively. From Fig. 1(b), we can see that the difference between the auto- and cross-correlation peaks for an incoherent system is much smaller than that obtained for the SIK system. Although sparse optical orthogonal codes (OOCs) can be applied to reduce that difference, they are only pseudoorthogonal and long code length and small code weight must be utilized, which reduces the spectral efficiency of the systems. In [12], an SIK optical CDMA was demonstrated; however, it was still based on balanced detection.

In our proposed approach, an all-optical SIK encoding/decoding scheme is implemented based on optical phase modulation and phase modulation to intensity modulation conversion by using FBG-based frequency discriminators. At the transmitter, instead of using optical intensity modulation, a low-bit-rate data sequence modulates the phases of the output of a laser diode (LD) array, and is then wavelength-mapped temporally to a high-bit-rate optical phase sequence via an FBG-array encoder. At the receiver, the second FBG array is used, which has two functions: 1) each FBG in this array acts as a frequency discriminator to convert the received phase-modulated optical signal to intensity-modulated signal and 2) the entire FBG array has a similar spectral property as that of the encoder FBG array but is connected in a time-reversed way; thus, it functions as a matched filter to decode the received optical signals. Bipolar decoding is achieved by placing the optical carriers at either the positive or the negative slopes of the reflection spectra of the FBGs in the decoder FBG array, owing to the feature that the recovered electrical signals from the opposite slopes have a π phase difference. Since the encoding is unipolar and the decoding is bipolar, the proposed scheme is equivalent to an SIK CDMA. Theoretical analysis and experimental results show that this approach has the potential to provide better performance than an incoherent implementation, and a simpler architecture than a bipolar modulation/balanced detection scheme.

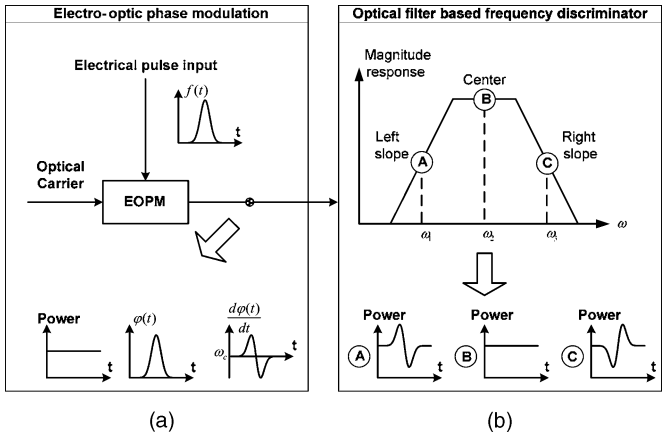

Fig. 2. Electrooptic phase modulation and its conversion to intensity modulation using an optical-filter-based frequency discriminator.

II. Principles

A. FBG-Based Frequency Discrimination

Since the EOPM and the FBG-based frequency discriminators are the key components in our proposed SIK CDMA, we first discuss the properties of the electrooptic phase modulation and its conversion to intensity modulation by using an FBG as a frequency discriminator.

In general, the normalized phase-modulated optical field $E_{PM}(t)$ can be expressed as

$$E_{PM}(t) = \exp[j\omega_c t + \varphi(t)] = \exp[j\omega_c t + \beta_{PM} f(t)] \quad (1)$$

where ω_c is the angular frequency of the optical carrier, $\varphi(t)$ is the phase change induced by the modulating signal,β_{PM} is the phase modulation index, and $f(t)$ is the electrical modulating signal. As can be seen from Fig. 2(a), the phase change of the optical carrier at the output of the EOPM is proportional to the amplitude of the modulating signal $f(t)$; and its first-order

derivative with respect to time t is the instantaneous frequency shift of the optical carrier, which is proportional to the amplitude of $f'(t)$, where $f'(t)$ denotes the first-order derivative of $f(t)$. If this phase-modulated optical signal is directly fed to a PD, the modulating signal cannot be recovered, but only a dc component will be obtained because the phase modulation does not change the envelope of the optical carrier and a PD functions as an envelope detector. However, if a frequency discriminator is placed after the EOPM, as shown in Fig. 2(b), PM-IM conversion is consequently realized. An ideal frequency discriminator is usually an optical filter that has two linear slopes and one flat top in its frequency response.

Mathematically, the frequency response of the optical filter shown in Fig. 2(b) can be written as (2) shown at the bottom of page, where K_1 and K_3 are, respectively, the slope steepness factors of the left and right slopes, and ω is the instantaneous optical frequency. To simplify the derivation, we assume that within each section the phase response is linear too. In the later part of this section, both the magnitude and phase responses of the proposed optical filter, i.e., an FBG, will be taken into account to carry out numerical simulations. Both the simulation results and the experimental results shown in Section III will prove that the assumption is acceptable by properly choosing the FBG fabrication parameters. In addition, we assume that the phase-modulated optical signal has a narrow bandwidth, and the optical carrier is selected such that its spectrum be totally located within each spectral section of the optical filter, as shown in Fig. 2(b).

After the optical signal described in (1) passes through the optical filter within one of those three sections and is fed to a PD, we can obtain the photocurrent at the output of the PD, which is given by

$$i_{PD}(t) \sim \begin{cases} dc|_{\omega_c=\omega_1} + K_1\beta_{PM}f'(t), & \text{left slope} \\ dc|_{\omega_c=\omega_2}, & \text{center} \\ dc|_{\omega_c=\omega_3} + K_3\beta_{PM}f'(t), & \text{right slope} \end{cases} \tag{3}$$

where the first term on the right-hand side for each case represents a dc current and can be eliminated by using a dc blocker. If the two slope steepness factors have identical magnitude but only different signs ($K_1 = -K_3 = |K|$), the recovered RF signal after the dc blocker can be written as

$$r(t) \sim \begin{cases} |K|\,\beta_{PM}f'(t), & \text{left slope} \\ 0, & \text{center} \\ -|K|\,\beta_{PM}f'(t), & \text{right slope} \end{cases} \tag{4}$$

Observing (4), we can conclude as follows.

1) No signal can be recovered if the optical carrier is located at the passband center of the optical filter, because the optical filter will neither change the phase nor the amplitude relationships among all the frequency components of the phase-modulated optical signal.
2) The recovered signal is proportional to the first-order derivative of the modulating signal when the optical carrier is located at either slope of the optical filter.
3) The obtained signals are π out of phase when the carriers are located at the opposite slopes.

The first feature will be used to realize the wavelength-temporal encoding in a unipolar way, and the last two features will be used to achieve the bipolar decoding in our proposed system.

FBGs are employed to realize the frequency discrimination in our proposed system for the following reasons. First, FBGs have been widely used to control and modify the amplitude and phase spectra of signals transmitted in fiber optical systems. In particular, for CDMA systems, FBG array (multiple FBGs fabricated in a single fiber but physically separated) can easily achieve wavelength-temporal coding scheme due to its "first in line, first reflected" feature [13]. Second, very sophisticated filter frequency responses can be achieved by manipulating the fabrication parameters during the FBG writing process, which makes the proposed frequency discriminator with an optimized frequency response possible [14], [15]. Third, the reflection wavelength can be tuned via changing the grating pitch by applying strain or varying temperature, thus, allowing for programmable encoding and decoding [4], [13].

Based on the above theoretical analysis, we know that the steepness and the width of the slopes determine the overall conversion efficiency and operational signal bandwidth, while both the reflectivity and phase response at the slopes should be linear, and any nonlinearity will introduce distortions to the recovered electrical signal. Therefore, the fabrication parameters of the FBG such as grating length, refractive index modulation depth, and apodization profile should be properly determined to obtain an optimized system performance. Basically, a strong FBG usually has a longer length or larger refractive index variation compared with a weak FBG, which can provide higher conversion efficiency and a flat top but a narrower transition bandwidth [15]. For the FBGs having identical lengths and refractive index variations, apodization will then play an important role in the FBG design to find out the best compromise between the system conversion efficiency and the linearity. In our numerical simulations, FBGs with uniform and Gaussian profiles are evaluated to understand the effects of apodization on the performance of the proposed frequency discriminator.

Based on the standard coupled-mode equations [15], a grating is divided into many short segments and the fundamental matrices for each segment are multiplied to obtain its overall characteristics. Fig. 3 shows the amplitude reflectivity and phase responses of two FBGs with an identical length of 10 mm, an average index change of 0.0001; but one has a uniform profile while the other one is Gaussian apodized. A Gaussian profile

$$|H(j\omega)| = \begin{cases} |H(j\omega)||_{\omega=\omega_1} + K_1 \cdot (\omega - \omega_1), & \omega_1 \text{ is located at the left slope} \\ |H(j\omega)||_{\omega=\omega_2}, & \omega_2 \text{ is located at the center} \\ |H(j\omega)||_{\omega=\omega_3} + K_3(\omega - \omega_3), & \omega_3 \text{ is located at the right slope} \end{cases} \tag{2}$$

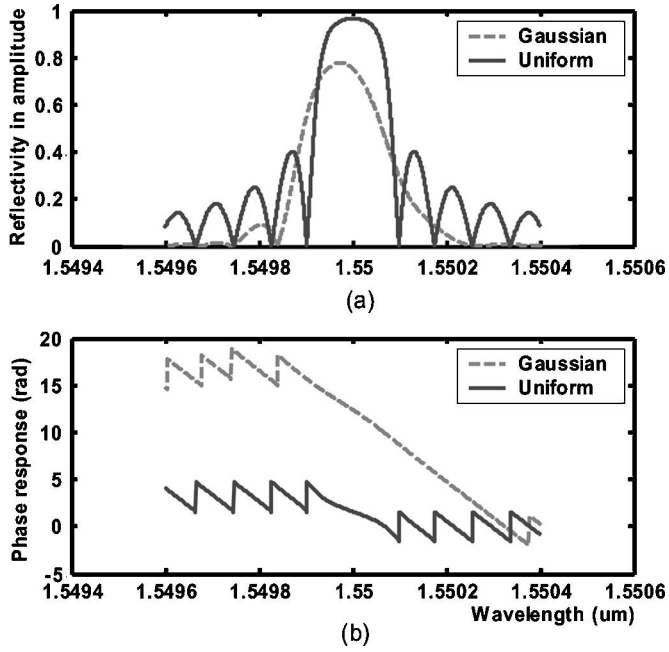

Fig. 3. Simulated reflectivity and phase responses. a) Uniform FBG. b) Gaussian-apodized FBG.

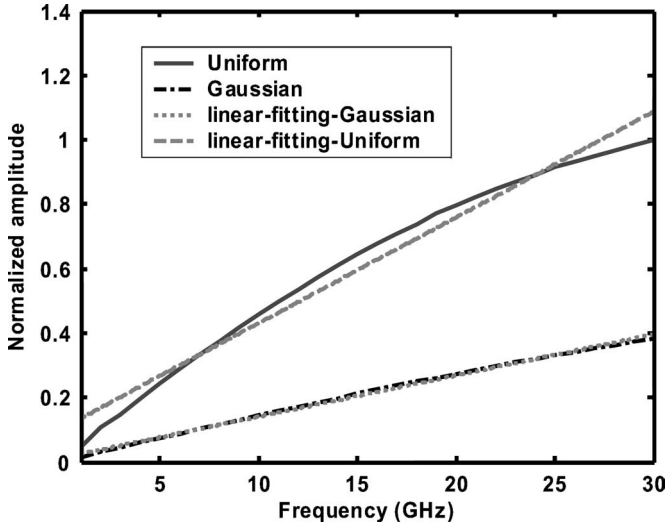

Fig. 4. Frequency responses (with respect to the modulating signal frequency) of the proposed frequency discriminators using a uniform and a Gaussian-apodized FBG.

can be expressed as

$$A(z) = \exp\left\{-\ln 2\left[\frac{2(z-L/2)}{sL}\right]^2\right\} \tag{5}$$

where $A(z)$ represents the average refractive index change along the grating length L as the function of the propagation distance z along the fiber, and s is the taper parameter. In this simulation example, the Gaussian taper factor is selected to be 0.25. The results show that if no apodization is applied, the wings of the grating will act similar to a Fabry–Perot cavity and strong resonance will be observed, which results in rapid fluctuations and nonlinearity of its reflectivity and phase responses. Employing Gaussian apodization, a significant suppression of the sidelobes is achieved, with very smooth rolling off slopes observed. In addition, the phase response is more linear than that of the uniform FBG. Based on the chosen FBGs, normalized magnitude responses of the proposed frequency discriminators with respect to the modulating signal frequency are further calculated, which are shown in Fig. 4. Owing to the FBG apodization, a good linearity and a wide operational bandwidth are obtained. It is to be noted that this is achieved at the cost of a lower PM-IM conversion efficiency.

B. SIK Optical CDMA

A point-to-point link of the proposed SIK (unipolar-bipolar) optical CDMA network is shown in Fig. 5. At the transmitter, an array of LDs is employed as a multiwavelength light source. Through an optical star coupler, the combined light beams are fed to an EOPM, which is driven by the preprocessed electrical signal that is expressed as

$$s(t) = \int_{-\infty}^{t} f(t)dt. \tag{6}$$

An array of N FBGs used as mirrors will perfectly reflect the N optical carriers at their reflection peaks to achieve code spreading. Either the input light wavelengths or the center wavelengths of the FBGs can be shifted relative to each other; hence, the individual chips of the coding sequence can be programmed to be either "1" (reflection) or "0" (no reflection), and can also be reconfigured. In fact, chip "0" can be easily realized by turning off the LD at the corresponding wavelength. Therefore, in a real system, the number of LDs can be less than the code length, which is determined by the weight of the coding sequence. Based on the first feature of the proposed frequency discrimination that the phase-modulated optical carrier being reflected at the FBG top can be considered to have no change, the encoded optical field is then written as

$$E_{\text{encod}}(t) = \sum_{n=1}^{N} \cos[\omega_{c,n}t + \beta_{PM}\, s(t - nT_c)]a_n \tag{7}$$

where $\omega_{c,n}$ represents the angular frequency of the nth carrier, a_n is the nth chip that takes on 0 or 1, and chip width T_c is determined by the round-trip optical path length between two adjacent FBGs.

At the receiver, an identical FBG array that is placed reversely is used as a matched filter. Each FBG in the decoder FBG array should have a central wavelength λ_n' slightly away from that (λ_n) of the corresponding encoder FBG. As shown in Fig. 5, whether the wavelength deviation should be toward the longer wavelength or shorter wavelength is determined by chip "-1" or chip "$+1$" required at the decoder. Then, the received optical signal will be reflected at the right or the left slopes of the decoder FBGs. Based on the second and the third features concluded previously for the FBG-based frequency discrimination,

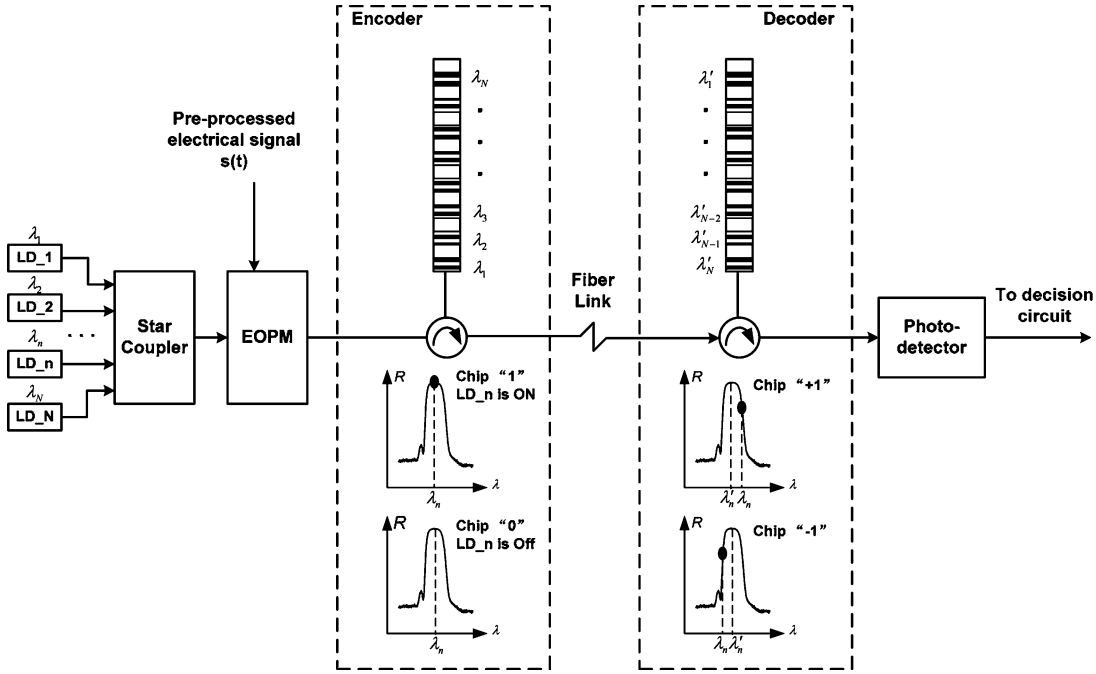

Fig. 5. Block diagram of a point-to-point link of the proposed SIK (unipolar–bipolar) optical CDMA system, where "dark point" in the inserts (with or without) represents the ON or OFF of the corresponding LD at the transmitter.

the PD output after the decoding can be written as

$$r_{\mathrm{decod}}(t) \sim \sum_{n=1}^{N} f(t - nT_c) a_n b_{N-n} \tag{8}$$

where $a_n \in (0,1)$ is the encoding signature from (7), and $b_{N-n} = 2a_{N-n} - 1, \in (-1,+1)$ is the decoding signature. Observing (8), it has the same expression as the correlation output of an SIK CDMA system [1], which can significantly reduce the cross-correlation peaks and eventually suppresses the MAI induced by other users.

III. Experiment

A. Frequency Discrimination Using a Gaussian-Apodized FBG

Based on the theoretical analysis and the simulations in Section II, an FBG is fabricated and its performance on optical frequency discrimination is evaluated. The FBG has a length of 10 mm, a peak power reflectivity of 99% (which is stronger than that of the FBG given in Fig. 3), and is Gaussian apodized. An additional complementary exposure without using the phase mask is implemented during the FBG fabrication process to make a Constant dc index change, to further suppress the sidelobes at the short-wavelength side. Its reflection spectrum is shown in Fig. 6(a), which has a center reflection wavelength at 1549.64 nm and a 3-dB bandwidth of 0.27 nm. A tunable laser with typical linewidth of 150 kHz is employed as the light source. Phase modulation is performed by using a $LiNbO_3$ straight-line phase modulator.

A 13.5 Gbit/s bit sequence with a fixed pattern as 10000000000000001... (15 consecutive "0"s between two "1"s) is generated by a bit-error-rate tester (BERT) to modulate the phases of the LD, which is equivalent to a pulse train with a repetition rate of 843.75 MHz and a duty-cycle of 1/16, as shown in Fig. 6(b) (top). Such an electrical pulse train is used to represent the data sequence in our experiments. A digital communication analyzer is used to monitor the output of the PD. An erbium-doped fiber amplifier (EDFA) is incorporated in the system to compensate for the system loss.

To verify the theoretical analysis presented in Section II-A, we tune the carrier wavelength such that it is reflected at different locations of the grating reflection spectrum, i.e., the left slope (A), the middle (B), and the right slope (C). Fig. 6(b) shows the waveforms of the corresponding electrical outputs. The experimental results clearly show that: 1) no signal can be recovered if the carrier is located at the center of the reflection band (point B); 2) when the carrier is located at the slopes (point A or C), the output is the first-order derivative of the modulating signal; and 3) the outputs obtained from the opposite slopes have a π phase difference. These observations agree well with the theoretical analysis and can be directly employed to achieving unipolar encoding and bipolar decoding in our proposed SIK optical CDMA.

B. Unipolar Encoding/Bipolar Decoding in OCDMA

To further verify the idea presented in Section II-B, two FBG arrays are fabricated using an ultraviolet (UV) light imprinting system. A translation stage with a maximum moving length of 200 mm and the step accuracy of 2 μm is used to scan the UV beam. The length of each grating and the distance between the adjacent gratings can be precisely controlled by using a computer to control the translation stage. A 130-mm-long uniform phase mask with a pitch of 1064 nm is used to write all the FBGs. The wavelength of each grating is very carefully controlled by controlling the tension applied to the fiber during the

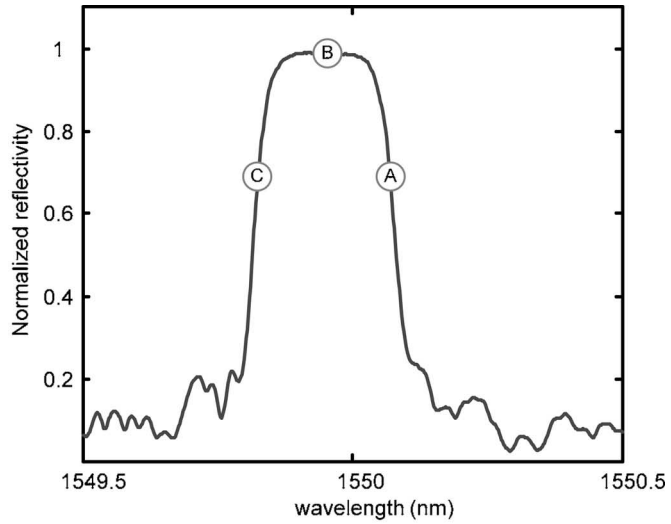

(a)

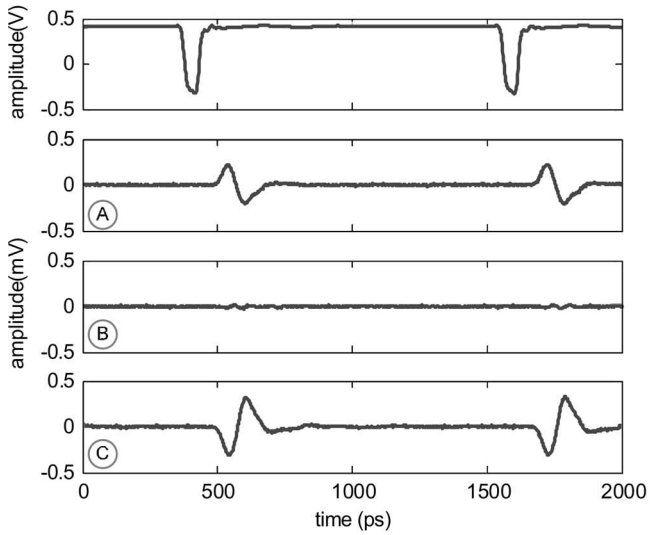

(b)

Fig. 6. a) Measured reflection spectrum of the FBG used in the experiment. b) Measured waveforms of the PD outputs when the optical carrier is located at different points: A, B, and C. The modulating signal is also recorded as a reference: top in (b).

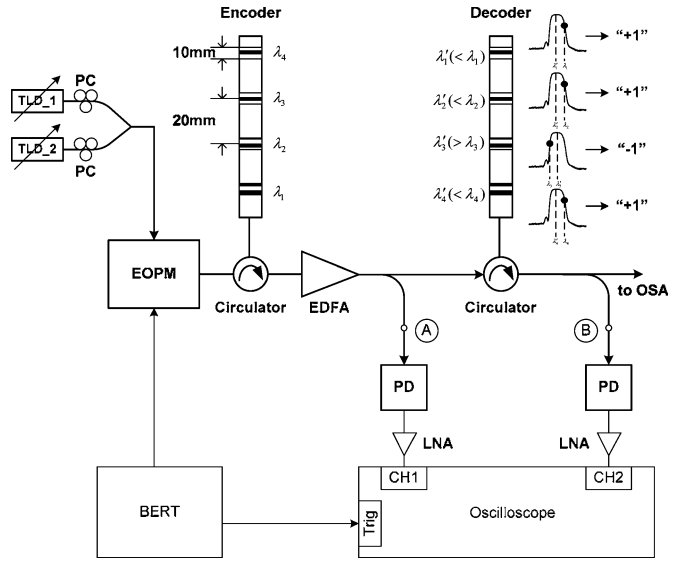

Fig. 7. Experimental setup of a point-to-point optical CDMA link.

photo-imprinting process. In this way, the Bragg wavelength can be shifted in a range of around 3 nm, which is sufficient for our experiment. Since only one phase mask is used to write FBGs in an array with different Bragg wavelengths, the alignment of the photo-imprinting system can be well maintained during the whole process, which is very important to obtain the FBGs with uniform performances. Each FBG array consists of four Gaussian-apodized FBGs corresponding to a code length of $N = 4$. Each FBG has a length of 10 mm and a reflectivity of 99%. The spacing between two adjacent FBGs is 20 mm, which gives a chip width of around 200 ps.

The experimental setup is shown in Fig. 7. At the transmitter, the outputs from two tunable LDs (corresponding to a code weight of 2) are combined by a 3-dB coupler and fed to an EOPM. The central wavelengths of the encoder FBGs are designated as a code vector $(\lambda_1, \lambda_2, \lambda_3, \lambda_4)$ with wavelength vector element λ_n being either "present" (chip "1") or "absent" (chip "0"). For instance, when the two LDs are tuned to λ_1 and λ_4, the encoder signature will be (1, 0, 0, 1). At the receiver, the central wavelengths of the decoder FBGs are designated as another wavelength code vector $(\lambda_4', \lambda_3', \lambda_2', \lambda_1')$ with wavelength vector element λ_n' being equal to either $\lambda_n + \Delta\lambda$ (chip "-1") or $\lambda_{N-n+1} - \Delta\lambda$ (chip "$+1$"), where $\Delta\lambda$ is a small deviation from the wavelengths of the encoder FBG array. Specifically, in our experiment, λ_1', λ_2', and λ_4' are slightly smaller than λ_1, λ_2, and λ_4, while $\lambda_3' > \lambda_3$. Consequently, the signature sequence in the decoder is $(+1, -1, +1, +1)$. We should mention here that the proposed scheme uses the wavelength as one of the coding factors. For the encoding code (1, 0, 0, 1), two laser diodes (corresponding to the two 0s) will be off. It results in a corresponding decoder signature, which should be (1, *, *, 1), where * can be either -1 or $+1$, without affecting the results.

In the matched case, when the two LDs are tuned at $\lambda_1 = 1546.55$ nm and $\lambda_4 = 1550.16$ nm, the signature sequences are, respectively, (1, 0, 0, 1) and (1, *, *, 1) in the encoder and the decoder. Fig. 8(a) and (b) show the optical spectrum and the corresponding electrical waveform of the encoded signal measured at point A by use of an oscilloscope. From Fig. 8(a), we can see that wavelength-temporal encoding is realized by reflecting the two phase-modulated optical carriers at two encoder FBGs with a time delay of 3 T_c. Since these two wavelengths are located at the centers of the encoder FBGs, no electrical pulses are observed [Fig. 8(b)].

Fig. 9 shows the optical spectra and electrical waveforms measured after decoding. To clearly explain the constructive generation of the correlation peak, results under two situations that one LD is on while the other one is off are also shown for comparison. From Fig. 9, we can obviously see that the electrical pulse (each oscilloscope screen shows two data bits) recovered from the FBG of λ_1' is constructively added to the pulse recovered from the FBG of λ_4' at the same time slot due to

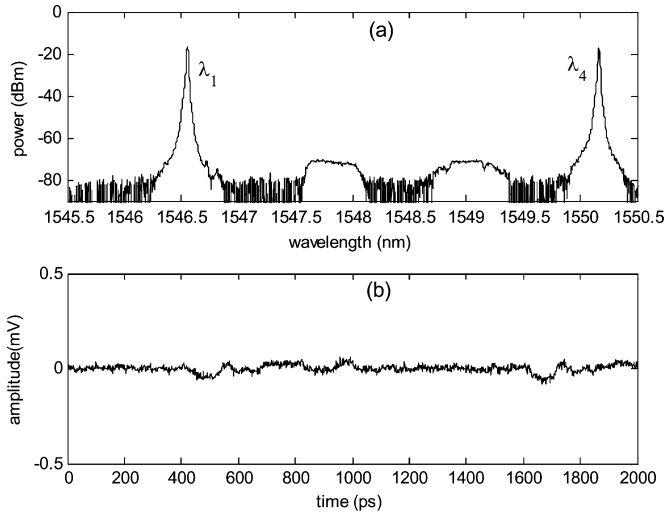

Fig. 8. (a) Measured optical spectrum after encoding. b) Corresponding electrical signal when wavelength vector (λ_1, λ_4) is selected.

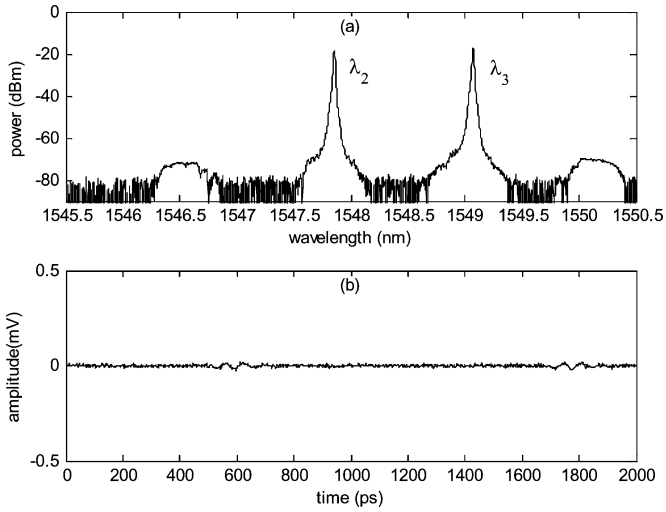

Fig. 10. a) Measured optical spectrum and b) the corresponding electrical waveform after the encoder, corresponding to the wavelength vector (λ_2, λ_3).

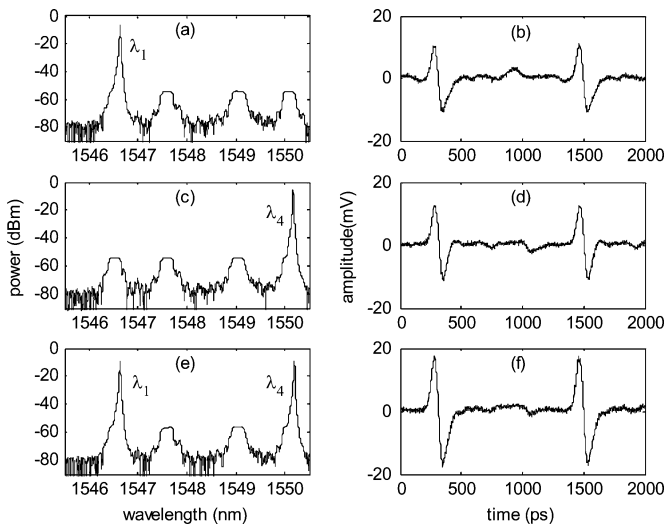

Fig. 9. Measurements obtained after decoding. a) LD at λ_1 is ON, LD at λ_4 is OFF. c) LD at λ_1 is OFF, LD at λ_4 is ON. e) Both LDs are ON. b), d), and f) are the observed electrical waveforms corresponding to (a), (c), and (e), respectively.

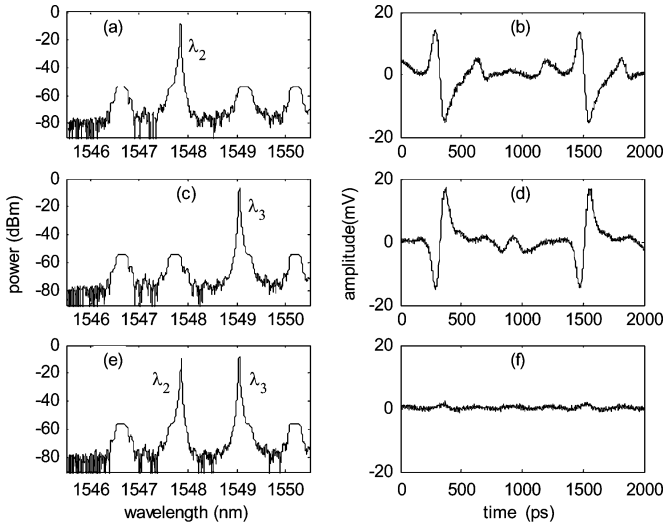

Fig. 11. Measurements obtained after decoding. a) LD at λ_2 is ON, LD at λ_3 is OFF. (c) LD at λ_2 is OFF, LD at λ_3 is ON. e) Both LDs are ON. b), d), and f) are the observed electrical waveforms corresponding to (a), (c), and (e), respectively.

the time-reverse connection of the decoder FBG array. Eventually, an autocorrelation peak is obtained. It should be noted that the recovered electrical pulse is the first-order derivative of the input data bit because no preprocess described by (6) is carried out in our experiment.

In the mismatched case, the signature sequences are, respectively, $(0, 1, 1, 0)$ and $(^*, -1, 1, ^*)$ at the encoder and the decoder, when the two LDs are tuned at wavelengths $\lambda_2 = 1547.85$ nm and $\lambda_3 = 1549.07$ nm. Again, the optical spectrum and the corresponding electrical signal after the encoder are measured as shown in Fig. 10(a) and (b). Fig. 11(a) and (b) show the optical spectra and the corresponding electrical signals obtained after decoding. We can see that the recovered signal from decoder grating λ_2' completely cancels out the signal recovered from the decoder grating λ_3', since they are out of phase. However, for a unipolar decoder with a signature sequence (*, 0, 1, *), a cross-correlation peak of 1 is expected. These results agree very well with the theoretical analysis in Section II and clearly verify that the proposed optical SIK can reduce the MAI effects compared with the unipolar–unipolar CDMA.

IV. Conclusion

An approach using a pair of all-optical encoder and decoder having equivalent performance as an SIK CDMA system was proposed and experimentally demonstrated in this paper. In the proposed system, an electrooptical phase modulator and two FBG arrays were employed to manipulate the optical code signature. At the transmitter, a low-bit-rate data sequence modulated the phases of the optical carriers by the EOPM, and was then wavelength-mapped temporally to a high-rate optical sequence by the encoder FBG array in a unipolar way. At the

receiver, a similar FBG array was employed to perform the frequency discrimination as well as matched filtering. Bipolar decoding was achieved by placing the optical carriers on either the positive or the negative slopes of the reflection spectra of the FBGs in the decoder FBG array. The proposed encoding/decoding scheme has the potential to provide improved performance than the conventional incoherent scheme using optical orthogonal codes. In addition, in an optical CDMA system using phase modulation, the intensity of the optical carrier remains constant, which is highly tolerant to the optical nonlinear effects such as self-phase modulation and cross-phase modulation. Moreover, compared with the bipolar decoder applying balanced detection, this approach has a simpler and more compact architecture. Furthermore, the proposed encoder/decoder can be quickly reconfigured by tuning either the wavelengths of the LDs or the central wavelengths of the FBGs. Experiments using a pair of FBG arrays to achieve unipolar encoding/bipolar decoding were demonstrated. The experimental results showed excellent agreement with the theoretical analysis. Some issues that affect the system performance should be addressed. First, the phase noise of each LD used at the transmitter will also be converted to intensity noise via the decoder FBGs. Second, the stability of the decoder outputs depends mainly on the wavelength stability of laser sources and FBGs. But if the relative wavelength shifts of the laser sources are still within the linear region of the FBGs reflection slopes, only the dc level of the output waveforms will be affected. The most critical requirement for the proposed system is to fabricate FBGs with linear slope, large dynamic range, and highly identical performance, which needs special efforts on FBG design and fabrication.

REFERENCES

[1] M. J. Parham and C. Smythe and B. L. Weiss, "Code division multiple-access techniques for use in optical-fiber local-area networks," *J. Electron. Commun. Eng.*, pp. 203–212, Aug. 1992.

[2] P. R. Prucnal, M. A. Santoro, and T. R. Fan, "Spread spectrum fiber-optic local area network using optical processing," *J. Lightw. Technol.*, vol. LT-4, no. 5, pp. 547–554, May 1986.

[3] J. A. Salehi, "Code division multiple-access techniques in optical fiber networks-part I: Fundamental principles," *IEEE Trans. Commun.*, vol. 37, no. 8, pp. 824–833, Aug. 1989.

[4] D. B. Hunter and R. A. Minasian, "Optical programmable high-speed optical code recognition using fiber Bragg grating arrays," *Electron. Lett.*, vol. 35, no. 5, pp. 412–414, Mar. 1999.

[5] L. R. Chen, S. D. Benjamin, P. W. E. Smith, and J. E. Sipe, "Applications of ultrashort pulse propagation in Bragg gratings for wavelength division multiplexing and code-division multiple-access," *IEEE J. Quantum Electron.*, vol. 34, no. 11, pp. 2117–2129, Nov. 1998.

[6] I. Andonovic, L. Tancevski, M. Shabeer, and L. Bazgaloski, "Incoherent all-optical code recognition with balanced detection," *J. Lightw. Technol.*, vol. 12, no. 6, pp. 1073–1080, Jun. 1994.

[7] C. F. Lam, D. T. K. Tong, M. C. Wu, and E. Yablonovitch, "Experimental demonstration of bipolar optical CDMA system using a balanced transmitter and complementary spectral encoding," *IEEE Photon. Technol. Lett.*, vol. 10, no. 10, pp. 1504–1506, Oct. 1998.

[8] I. Andonovic, L. Tancevski, M. Shabeer, and L. Bazgaloski, "Incoherent all-optical code recognition with balanced detection," *J. Lightw. Technol.*, vol. 12, no. 6, pp. 1073–1080, Jun. 1994.

[9] C. F. Lam, D. T. K. Tong, M. C. Wu, and E. Yablonovitch, "Experimental demonstration of bipolar optical CDMA system using a balanced transmitter and complementary spectral encoding," *IEEE Photon. Technol. Lett.*, vol. 10, no. 10, pp. 1504–1506, Oct. 1998.

[10] S. J. Kim, T. Y. Kim, C. S. Park, and C. S. Park, "10-Gb/s temporally coded optical CDMA system using bipolar modulation/balanced detection," *IEEE Photon. Technol. Lett.*, vol. 17, no. 2, pp. 510–512, Feb. 2005.

[11] M. B. Pursley, *Spread-Spectrum Multiple-Access Communications in Multi-User Communication Systems*, G. Longo, Ed. New York: Springer-Verlag, 1981.

[12] T. O Farrell and S. Lochmann, "Performance analysis of an optical correlator receiver for SIK DS-CDMA communication system," *Electron. Lett.*, vol. 30, no. 1, pp. 63–65, Jan. 1994.

[13] H. Fathallah, L. A. Rusch, and S. LaRochelle, "Passive optical fast frequency-hop CDMA communications system," *J. Lightw. Technol.*, vol. 7, no. 3, pp. 397–405, Mar. 1999.

[14] K. O. Hill and G. Meltz, "Fiber Bragg grating technology fundamentals and overview," *J. Lightw. Technol.*, vol. 15, no. 8, pp. 1263–1276, Aug. 1997.

[15] T. Erdogan, "Fiber grating spectra," *J. Lightw. Technol.*, vol. 15, no. 8, pp. 1277–1294, Aug. 1997.

Fei Zeng (S'04–M'07) received the B.Eng. degree in optoelectronic engineering from Huazhong University of Science and Technology, Wuhan, China, in 1993,and the M.A.Sc. and Ph.D. degrees in electrical engineering from the School of Information Technology and Engineering, University of Ottawa, Ottawa, ON, Canada, in 2003 and 2006, respectively.

From 1993 to 2001, he was with NEC Fiber Optical Communications Ltd, Wuhan, China, working on synchronous digital hierarchy and dense wavelength-division multiplexing system verification. He is currently with the Research Laboratory of Electronics, Massachusetts Institute of Technology, Cambridge. His research interests include microwave photonics, and photonic nanostructures for biosensing, nanomanipulation, and biospectroscopy.

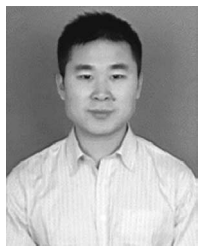

Qing Wang received the Bachelor's degree in electronic engineering and Ph. D degree in electronic science and technology from Tsinghua University, Beijing, China, in 2000 and 2006, respectively.

Since March 2006, he has been with the Microwave Photonics Research Laboratory, School of Information Technology and Engineering, University of Ottawa, Ottawa, ON, Canada, as a Postdoctoral Researcher. His research interests include fiber amplifiers and lasers, fiber Bragg gratings, nonlinearities in fiber- and semiconductor-based optical devices, and microwave photonic signal generation and processing.

Jianping Yao (M'99–SM'01) received the Ph.D. degree in electrical engineering from the Université de Toulon, Toulon, France, in 1997.

From 1999 to 2001, he held a Faculty position with the School of Electrical and Electronic Engineering, Nanyang Technological University, Nanyang, Singapore. He joined the School of Information Technology and Engineering, University of Ottawa, Ottawa, ON, Canada, in 2001, where he is currently a Professor and the Director of the Microwave Photonics Research Laboratory. He is a Guest Professor with Shantou University, Shantou, Guangdong, China, and Sichuan University, Chengdu, Sichuan, China. He was an Invited Professor with the Institut National Polytechnique de Grenoble, Grenoble, France, in 2005. His research interests include fiber lasers, fiber-optic sensors, biophotonics, and microwave photonics. He is the author of over 150 papers published in refereed journals and conference proceedings.

Dr. Yao is a member of the International Society for Optical Engineers and the Optical Society of America.